Capabilities of anion and cation on hydrogen-bond transition from the mode of ordinary water to (Mg, Ca, Sr)(Cl, Br)$_2$ hydration

Hengxin Fang[1], Zhixu Tang[1], Xinjuan Liu[2], Yongli Huang[1,*] Chang Q Sun[3,4,*]

Abstract

It has been a long pursuit to discriminate the ionic roles of mono- and di-valent salt solutions in modulating the hydrogen bonding network and solution properties. We attended this issue by examining the effect of concentrated YX_2 (Y = Mg, Ca, Sr; X = Cl, Br) solvation on O:H–O bonds transition from the mode of ordinary water to hydration in terms of the number fraction $f_{YX2}(C)$ and the segmental O:H–O bond phonon stiffness shift $\Delta\omega(C)$ with C being the solute concentration. The invariant $df_Y(C)/dC$ coins that the small Y^{2+} forms a constantly-sized hydration droplet with weak responding to interference of other ions because its hydrating H_2O dipoles screen mostly its electric field. However, the number inadequacy of the highly-ordered hydration H_2O dipoles partially screens the large X^-. The $X^- \leftrightarrow X^-$ electrostatic repulsion exists and weakens its electric field. The concentration-trend consistency of the $f_{YX2}(C)$, the solution conductivity $\sigma_{YX2}(C)$, and surface stress (contact angle) $\theta_{YX2}(C)$ for YX_2 solutions clarifies their common origin of ionic polarization. However, the Jones–Dole notion disobedience of the viscosity $\eta_{YX2}(C)$ suggests the presence of Y^{2+}~X^- electrostatic attraction.

[1] Key Laboratory of Low-dimensional Materials and Application Technology, School of Materials Science and Engineering, Xiangtan University, Xiangtan 411105, China (fhx18942929172@163.com; tangzhixv@163.com; huangyongli@xtu.edu.cn)

[2] CBME, China Jiliang University, Hangzhou 310018, China (14A050288@cjlu.edu.cn)

[3] EBEAM, Yangtze Normal University, Chongqing 408100, China (ecqsun@gmail.com)

[4] NOVITAS, Nanyang Technological University, Singapore 639798 (ecqsun@ntu.edu.sg)

Content entry

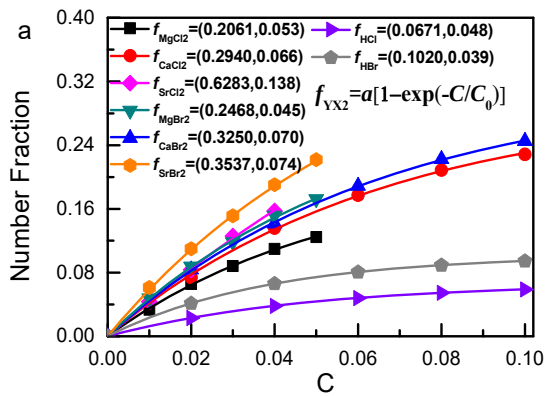

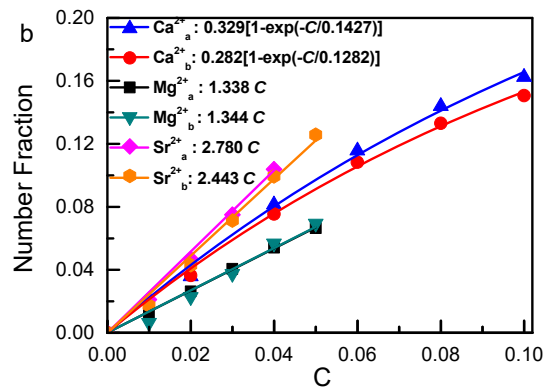

Illustration (to referees):

Resolved Y^{2+} and $2X^-$ capabilities of transiting the fraction of O:H-O bonds from ordinary water to hydration, which fingerprints the hydration shell sizes, ionic fields and correlate to the solution conductivity and surface stress. The Jones–Dole notion disobedience of the viscosity $\eta_{YX2}(C)$ suggests the presence of Y^{2+}~X^- electrostatic attraction.

1. Introduction

Salt solvation is ubiquitously important to our living quality and research fields such as environmental engineering [1-2], medicine industry [3], food science and technology [4-5], metallurgical engineering [6-8] and construction materials [9]. The solvation of a divalent salt has striking impact on the biochemistry, organic chemistry, food and medicine, and health care of human beings [10-11], which modulate not only the surface stress and viscosity of the solutions but also changes the solution ability of biological molecules such as denature of DNA and dissolving proteins. The interaction between salt ions and water molecules play a critical role in mediating the structure and property of solvent water. It has been a flourishing subject of research since the Hofmeister series was initiated [12], however, high-resolution and clarification of solute-solvent molecular interaction remain yet mysterious.

Compared with the monovalent salt solution at a certain centration C, a divalent salt solution has Y^{2+} and folded-number of X^- at the same concertation, which "hardens" drinking water and is unhealthful to us[13-14]. Spectroscopic investigation has been made on the dipole orientation and interface dielectrics [14], hydration network relaxation upon solvation [15], the molecular and solute diffusion dynamics in terms of phonon lifetime [16]. Amazing variations have been observed on the hydrogen bond network structure [14], orientation dynamics of water molecules [17], as well as the phonon lifetime and frequency shift of the H–O bond in H_2O or HDO solutions [16, 18]. It is expected that the size, polarity, and electronegativity of ions have different roles on the surrounding water molecules leading to salting in or salting out proteins in aqueous solutions ranked by Franz Hofmeister.

Halides participate in various biochemical processes [19-20]. For instance, the chlorine anion stabilizes cells at a proper osmotic pressure. Calcium, magnesium and manganese cations play an essential role in biological system [2122-24]. The X-ray absorption spectrum of chloride aqueous solutions suggested that the observed spectral changes of monovalent chloride solutions are primarily responsible for the water-chloride interactions, but the spectral variations of divalent chloride solutions result from the strong interactions between the dissolved cations and water molecules in the first hydration shell [25].

For instance, Jong and Neilson [26] investigated the hydration of the concentrated nickel chloride solutions with variation of temperature and pressure and found that the Ni^{2+} and Cl^- hydration shells become progressively weak at elevated temperature. Combining neutron diffraction and Monte Carlo simulation, Bruni [14] suggested that the electrostatic field raised from divalent cations dictates the strong and directional interactions with water molecules in the first hydration shell and forms a more rigid and long lasting hydration shell (called supersolidity [27]), compared with the monovalent ionic solutions. The interaction between various halides ions and water molecules, but discriminating the divalent cations from the monovalent ions in the hydration mechanisms remains a challenging issue. Consistent understanding of the solute-solute and solute-solvent interactions of the dissolved divalent cations, halides anions, and water molecules would be helpful.

We show here the progress of the concerned issues by examining the O:H–O bond transition from the mode of ordinary water to hydration by divalent halide solvation in terms of phonon abundance and stiffness and the correlation between the surface stress, viscosity and conductivity pf the solutions.

2. Experimental Section

The analytical reagents of $MgCl_2$, $CaCl_2$, $SrCl_2{\cdot}6H_2O$, $MgBr_2{\cdot}6H_2O$, $CaBr_2$ and $SrBr_2{\cdot}6H_2O$ were purchased from the Aladdin Industrial Inc. Deionized water was produced by a HITECH laboratory water purification system (resistivity: 18.2 MΩ·cm). Raman measurements of 150 μL deionized water and aqueous solutions injected into a silica stage were conducted using the confocal micro Raman spectrometer (Renishaw inVia) with a 532 nm He–Ne laser as the light source at the ambient pressure and 298 K. All the measurements were conducted in a back-scattering geometry using a 50 × long-working-distance objective lens (Leica) to focus the laser light onto the sample and collect the scatted light. The phonon frequency range, exposure time and accumulated number were set to 50-3800 cm^{-1}, 30 s, and 4, respectively. According to limit of the solubility, salt aqueous solutions were prepared at suitable solute molar fractions $C = N_{YX2}/N_{H2O}$. The contact angle detection was carried out by the Drop Sharp Analysis System (Krüss GmbH, Germany). The fluidic absolute viscosity and conductivity were measured by an NDJ-5S digital rotary viscometer with the No.0

rotor (Pingxuan Scientific Instrument Co., Ltd, China) and MP515-03 precision conductivity meter (Shanghai Sanxin Instrumentation, Inc), respectively.

3. Principles

3.1. Interlock of the tetrahedrally-coordinated YX_2 and H_2O networks

The YX_2 solution network is an interlock of the ordered, tetrahedrally-coordinated YX_2 and H_2O solutions. Figure 1a inset shows the $2H_2O$ unit cell of four identical O:H–O bonds linking neighboring oxygen atoms. As a basic structure and energy-exchange unit, the O:H–O bond couples the intermolecular O:H nonbond and the intramolecular H–O polar-covalent bond interactions through the O–O repulsion, rather than either the O:H or the H–O alone. The H–O bond releases/absorbs energy and the O:H nonbond relaxation dissipates energy through the motion of H_2O molecules. The O:H–O is regarded as an asymmetrical, short-range, and strongly coupled oscillator pair [28] whose segmental length, cohesive energy and stretching vibration frequency for H–O bond are (1.0 Å, ~4.0 eV, 3200 cm^{-1}) and for O:H nonbond they are (1.7 Å, ~0.1 eV, 200 cm^{-1}) at 4 ºC and ambient pressure [29]. In pure water, the total number of protons and one pairs ":" and the O:H–O configuration conserve. The $2H_2O$ unit cell defines that any one of the molecules can only rotates around the C_{3V} symmetrical axis within 60°, or otherwise the H↔H and O:⇔:O repulsion will come into play to destabilize the hydrogen bonding network.

Figure 1b inset shows the proposed $2YX_2$ unit cell. The YX_2 dissolves into Y^{2+} and X^- ions and each of them serves as a center of electric field. Electrostatic polarization does not form any bonds of new kinds but only clusters, polarizes, and stretches the neighboring water molecules. Ions are screened by its surrounding H_2O molecules to form the supersolid hydration shells (inset of Figure 1c) – highly polarized, gel-like, thermally more stable [27]. The dissolved cations and anions form a homogeneous tetrahedral unit, which is like the $2H_2O$ with four identical Y^{2+}~X^- ~Y^{2+} electrostatic interaction. The smaller divalent Y^{2+} cations occupy the center and four vertices of the tetrahedron. Four larger X^- anions are located at the midpoint between two Y^{2+} cations, and bridges Y^{2+} cations through the cation-anion attraction. In the network, the Y^{2+}~X^- attraction and Y^{2+}↔Y^{2+} X^-↔X^-

repulsion coexists but the extent will be subject to the solute concentration and screening of the H_2O dipoles in the hydration shells.

The size, charge sign and quantity, electronegativity, concentration or separation between ions determine the strength of the solute ionic electric field. Ionic electrification shortens and stiffens the H–O bond but elongates and softens the O:H nonbond [27](see inset d). The O:H–O segmental length and vibration frequency fingerprints directly the local electronic fields as a superposition of the contributions from the point charges and the H_2O dipoles that screen the ions' electric fields.

3.2.Phonon spectroscopic identities

The Raman frequency shift $\Delta\omega_x$ fingerprints the relaxation of the segmental length d_x and energy E_x from one equilibrium to the next under any external perturbation [29],

$$\Delta\omega_x \propto \sqrt{E_x/\mu_x}/d_x \propto \sqrt{\frac{k_x + k_C}{\mu_x}}$$

The subscript X = L and H denotes the O:H nonbond and the H–O covalent bond, respectively. The μ_x is the reduced mass of the vibrating dimer; k_C and k_x are the force constants, or the curvatures of the O–O Coulomb repulsion and the respective segmental potential.

The Raman full-frequency spectra compared in Figure 1 characterizes the O:H–O bond cooperative relaxation upon YX_2 solvation, which hardly offer quantitative information on the stiffness, abundance and fluctuation-order transition of the O:H–O bond by solvation. The differential phonon spectrometrics (DPS)[28], however, can distill such information very conveniently. The DPS is obtained by subtracting the referential spectrum of deionized water from the spectrum of the solution upon both spectral peaks being area normalized. Ref [27] has described the DPS strategy in detail.

The DPS shows the phonon population transition from the valley to the peak above the x-axis Figure 2 and Figure 3, which corresponds to the number of bonds transiting from the mode of ordinary

water to hydration in the solute hydration shells. The integration of the peak features the number fraction $f_x(C)$ of bond transition due to polarization [27],

$$f_x(C) = \int_{\omega_m}^{\omega_M} \left[\frac{I_{solution}\ (C,\omega)}{\int_{\omega_m}^{\omega_M} I_{solution}\ (C,\omega) d\omega} - \frac{I_{water}\ (0,\omega)}{\int_{\omega_m}^{\omega_M} I\ _{water}\ (0,\omega) d\omega} \right] d\omega$$

The slope of $f_x(C)$ is proportional to the population of bonds per set of $Y^{2+} + 2X^-$ solutes, which reflects the hydration shell sizes determined by its local electric field of the solutes. In the present case, the $f_x(C)$ is the superposition of $f_Y(C) + f_{X2}(C) = f_{YX2}(C)$. The fraction coefficient $f_Y(C)$ and $f_{X2}(C)$ may be linear, or nonlinear of different curvatures $d^2f_x(C)/dC^2$, which features how the local electric filed changes with the local bonding environment and solute concentration. The $f_x(C) = 0$ means no polarization occurs, such as H^+ in acid solutions [30]; $df_x(C)/dC = 0$ indicates invariant hydration shell size of Na^+, Li^+, and K^+ in monovalent salt solutions; and $d^2f_x(C)/dC^2 > 0$ or < 0 features the dominance of inter-solute attraction or repulsion, respectively [27].

4. Results and Discussion

4.1. Raman Spectral Characteristics

Figure 1 compares the full-frequency (50–3800 cm^{-1}) Raman spectra of YX_2 solutions. One should focus on the cooperative relaxation of the O:H nonbond stretching vibration ω_L at 50–300 cm^{-1} and the H–O bond stretching vibration ω_H at 3100–3800 cm^{-1}. Salt solvation shifts the O:H and the H–O phonon cooperatively without adding any new features of bond formation. Solvation of the YX_2 stiffens the H–O phonon and softens the O:H phonon simultaneously without being able to discrimination of the $2X^-$ from the Y^{2+} contribution. The spectral features within 300-3000 cm^{-1} range due to bond angle bending and rotating vibration are out of immediate concern as it fingerprints less the change of segmental length and energy. This is the advantage of the phonon spectroscopy based on the Fourier transition scheme that sorts out the bonds vibrating in the same frequency disregarding the orientation and or location.

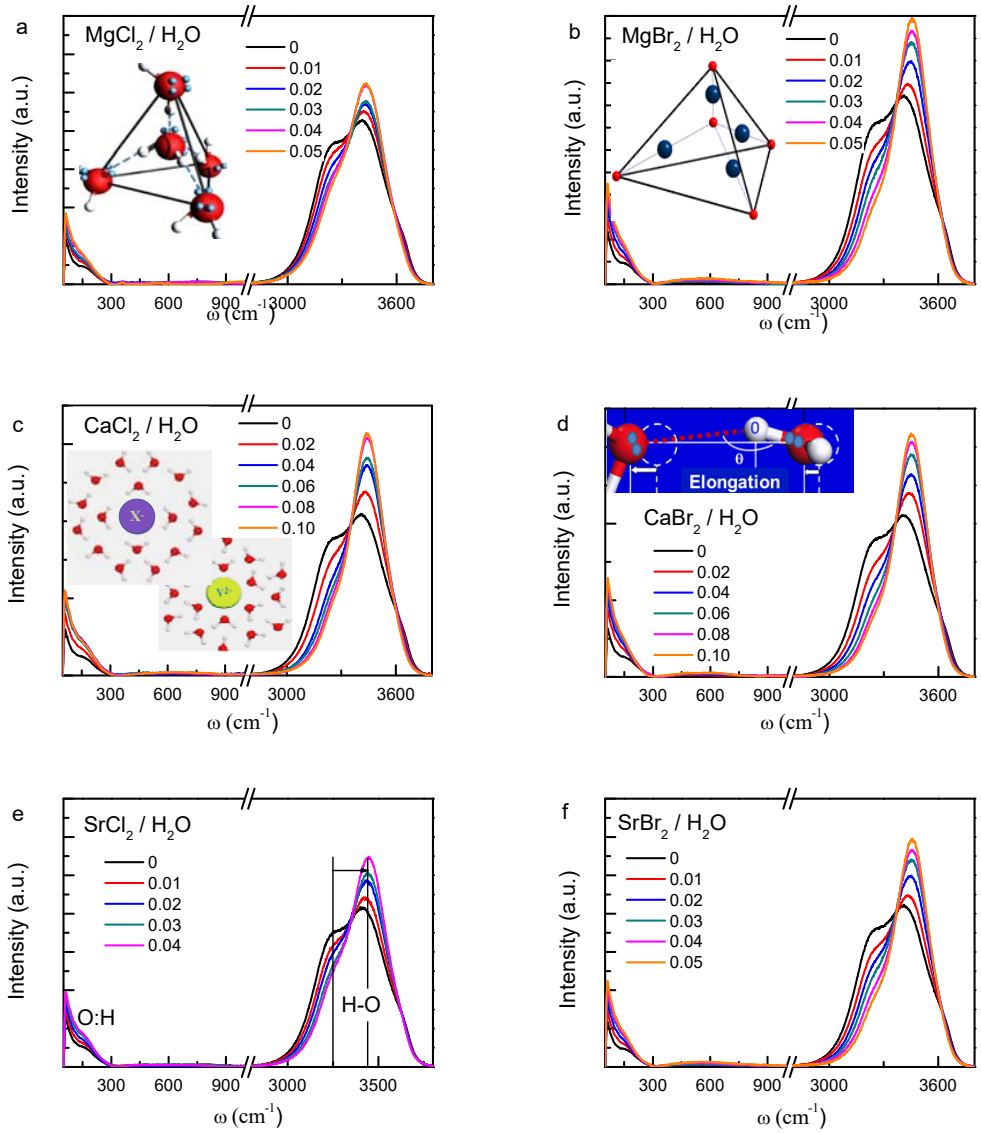

Figure 1. Full-frequency Raman spectra of (Mg, Ca, Sr)(Cl, Br)$_2$ solutions. Inset a illustrates the $2H_2O$ structural unit cell comprising four oriented O:H–O bonds with pairing dots standing for the lone pairs ":" on oxygen. Inset b illustrates the $2YX_2$ unit cell extending from the $2H_2O$ by removing the ":". Inset c illustrate the effect of Y^{2+} and X^- charge injection on water molecules aligning and clustering, and the (inset d) electric stretching of the O:H–O bond. The ionic sizes are R_Y ~1.0 Å for Y^{2+} and R_X ~2.0 Å for X^-. Inset e denotes frequency regimes of O:H and the H–O stretching vibrations and the shift $\Delta\omega_x$ as a function of the segmental length d_x and energy E_x. From the phonon frequency shift one can see directly the bond stiffness relaxation.

4.2. Bond stiffness cooperative transition

DPS of the concentrated YX_2 aqueous solutions showing the ionic polarization that shortens H–O bond and stiffens it phonon from 3200 cm^{-1} (valley) to ~ 3450 cm^{-1} (peak); the O:H nonbond responds to ionic polarization oppositely and its phonon shifts from ~200 cm^{-1} to ~ 110 cm^{-1} for YCl_2 and to ~100 cm^{-1} for YBr_2 solutions. The second valley at 3620 cm^{-1} corresponds to the dangling H–O vibration phonon stiffened from 3610 cm^{-1} by the X^- ions preferentially populated at the surface, whose intensity is annihilated by the anions. These features confirm the effect of polarization on H–O bond shortening and O:H softening. However, in the monovalent salt solutions, polarization transits the H–O phonon from 3200 to ~3500 cm^{-1} and the O:H phonon from 200 to ~75 cm^{-1}. The lower capability of polarization indicates the local weaker electric fields around the ions in the YX_2 solutions because of the superposition of the repulsion between the like ions and the attraction between the alike ions.

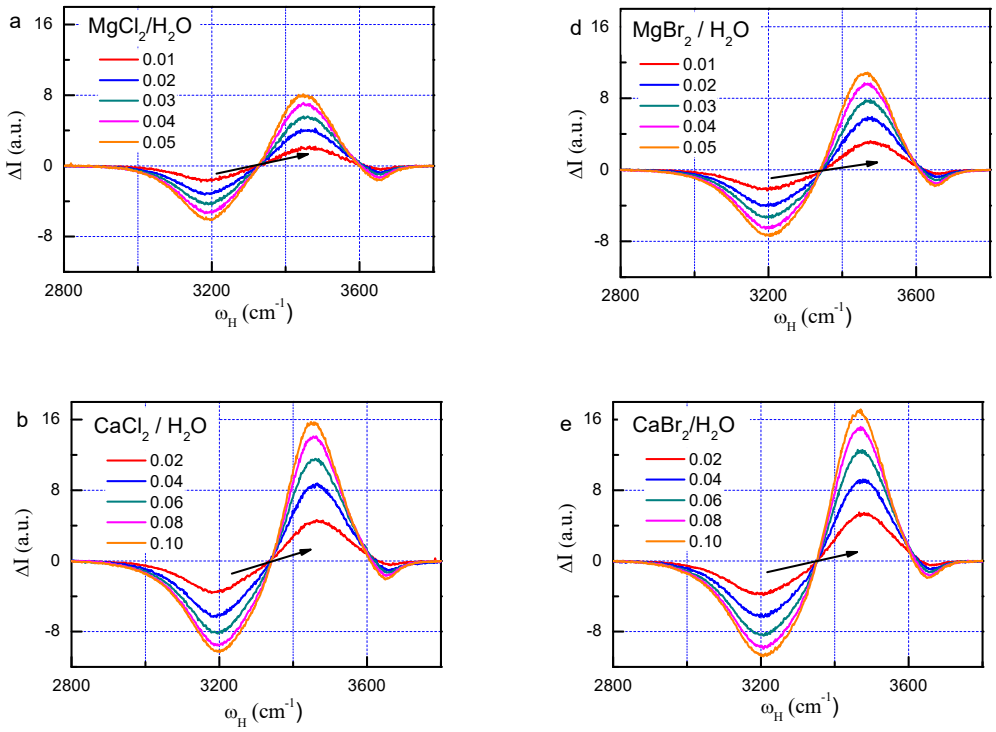

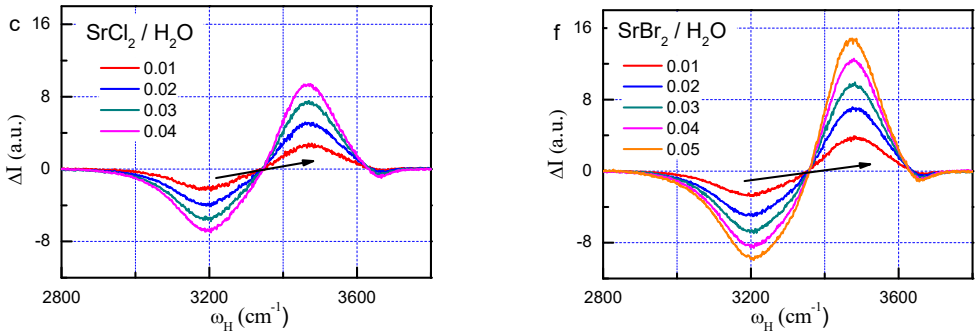

Figure 2. The H—O phonon DPS for the concentrated (Mg, Ca, Sr)(Cl, Br)$_2$ solutions. Aqueous charge injection transits the H–O bonds from the mode of ordinary water centered at 3200 cm^{-1} to the hydration states at ~3450 cm^{-1}, as consequence of H–O bond contraction and stiffening ($\omega_x^2 \propto E_x/d_x^2$).

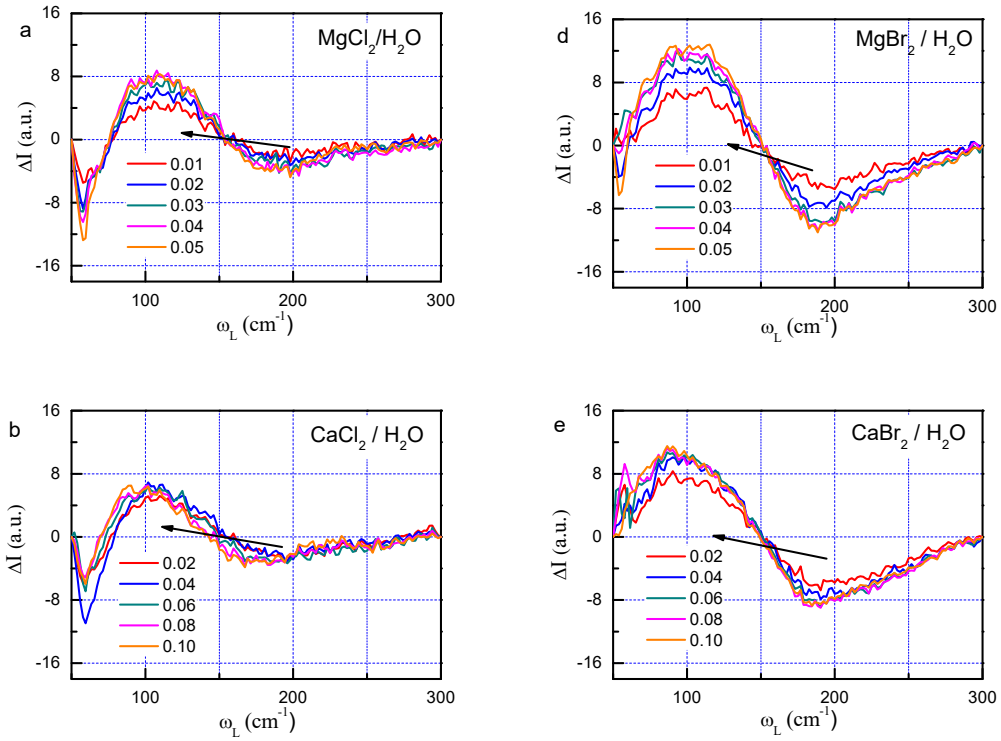

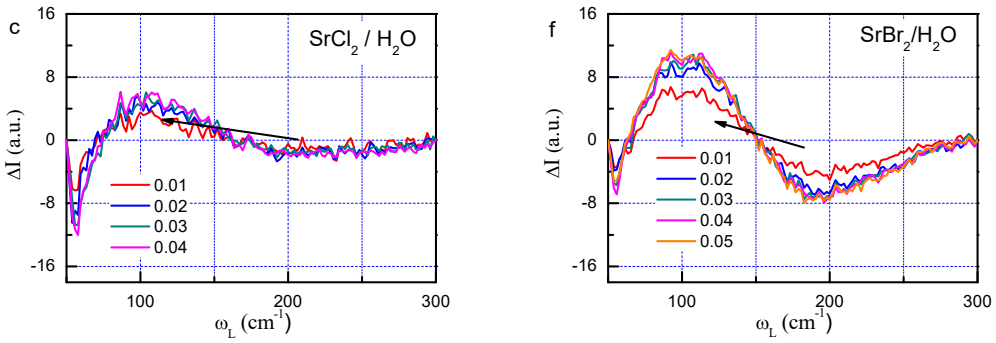

Figure 3. The O:H phonon DPS for the concentrated (Mg, Ca, Sr)(Cl, Br)$_2$ solutions. Aqueous charge injection transits the O:H nonbonds from the mode of ordinary water centered at 200 cm^{-1} to the hydration states at ~100 cm^{-1}, resulting from the O:H nonbond elongation and softening ($\omega_x^2 \propto E_x/d_x^2$).

4.3. Fraction of bond transition

Integration of the DPS H–O phonon peaks results in the fraction $f_{YX2}(C)$, which is the number of bonds transiting from the mode of water to hydration. It has been verified[30-33] that the $f_H(C) = 0$ and hence the $f_{HX}(C) \cong f_X(C)$ as the H^+ does not polarizes its surrounding O:H–O bonds. The excessive H^+ is attached to a H_2O to form H↔H anti-HBs between H_3O^+↔H_2O, which serves as point beaker to disrupt the local HB networks. Therefore, $f_X(C) \cong f_{HX}(C) - f_H(C)$. The X^- anion performs the same to polarize neighboring H_2O molecules to form the hydration shell. Therefore, $f_Y(C) \cong f_{YX_2}(C) - f_{HX}(2C)$, where the $f_{HX}(2C)$ represents the folded X concentration in the YX_2 solutions. The $f_Y(C)$ and $f_{X2}(C)$ can thus be separated from the $f_{YX2}(C)$. Figure 4 compares the $f_{YX2}(C)$, $f_Y(C)$, and $f_{X2}(C)$ for the concentrated YX_2 solutions.

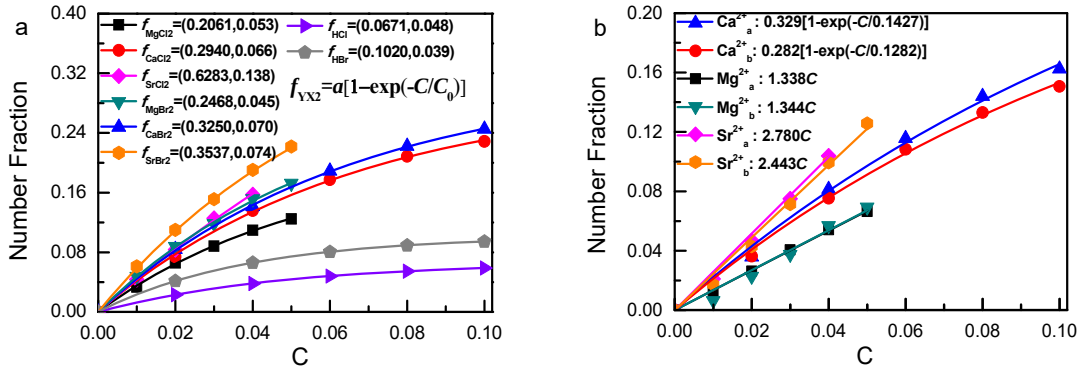

Figure 4. Comparison of (a) the present $f_{YX2}(C)$ and the $f_{HX}(C)$ for acid solutions[30] and (b) the $f_Y(C)$ for the divalent cations. The slopes and curvatures of the coefficients provide information on the ionic local electric fields and the hydration shell sizes as a function of concentration.

The six $f_{YX2}(C)$ profiles in the exponential saturation form are categorized in three groups in Figure 4a. Results show the ionic capabilities of O:H–O bond polarization follows the order: Sr^{2+} > Ca^{2+}> Mg^{2+} and Br^- > Cl^-. One can find that the $f_{YX2}(C)$ rises with the ionic size and with the drop of electronegativity [R(Mg^{2+}) = 0.49 Å, R(Ca^{2+}) = 0.99 Å, R(Sr^{2+}) = 1.12 Å: R(Br^-)= 1.96 Å, R(Cl^-) = 1.80 Å].

One can obtain the $f_{2x}(C) = f_x(2C)$ by twisting the C in the $f_{HX}(C)$ directly in Figure 4a. From the $f_{2x}(C)$ slope analysis, $X^-\leftrightarrow X^-$ repulsion remains throughout the concentrated solutions because the large X^- size [27]. Insufficient number of H_2O molecules in the highly-ordered hydration shells only partially screen the electric field of the X^- ions, being the same case of monovalent salt solutions.

Figure 4b shows that at $C \leq 0.05$, the $f_Y(C) \propto C$ and at higher C, the $f_Y(C)$ follows the same trend of $f_X(C) \propto 1 - \exp(-C/C_0)$ toward saturation. The subscript a and b legend the Y^{2+} in the YCl_2 solutions and the Y^{2+} in the YBr_2 solutions, respectively. The critical molecular ration C = 0.05 = 1/20 means that 20 H_2O molecules surround one set of Y^{2+} + $2X^-$ solutes. At such concentration or below, the Y^{2+} seems fully screened by its surrounding H_2O dipoles, and the $Y^{2+}\leftrightarrow Y^{2+}$ repulsion or the Y^{2+}-X^- attraction is negligible. However, at higher concentration, the $Y^{2+}\leftrightarrow Y^{2+}$ repulsion occurs because eof the shorter distance. However, the absence of $Y^+\leftrightarrow Y^+$ repulsion from the monovalent salt solutions

suggests that the Y^{2+} has a longer distance of its electric field. The Y^{2+} and the Y^{+} difference and the folded X^{-} number discriminate the monovalent and divalent salt solutions of the same concentration.

4.4. Solution conductivity, surface stress, and viscosity

Figure 5 compares the solution conductivity $\sigma_{YX2}(C)$ and surface stress (contact angle $\theta_{YX2}(C)$) of the solution. Strikingly, the $\sigma_{YX2}(C)$, $\theta_{YX2}(C)$ share the similar $f_{YX2}(C)$ exponential decay with increasing solute concentration. These identities follow the same order of the solutes: $Sr^{2+} > Ca^{2+} > Mg^{2+}$ and $Br^{-} > Cl^{-}$ as well. These concentration trend consistency evidences their common origin of polarization. The $\sigma_{YX2}(C)$ drop at higher concentration for the thicker solutions may arise from the carrier low mobility.

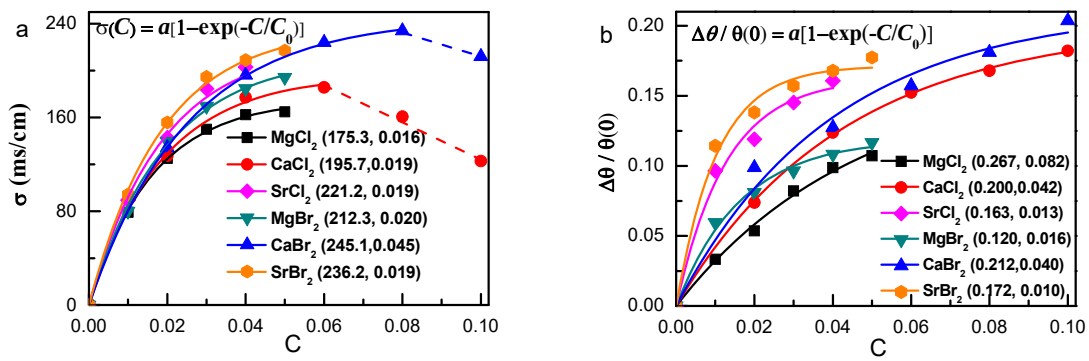

Figure 5. Solute concentration and type resolved (a) solution conductivity and (b) surface stress (contact angle) follow the same trend of exponential decay of the fraction coefficient toward situation and the capability order of the solutes: $Sr^{2+} > Ca^{2+} > Mg^{2+}$ and $Br^{-} > Cl^{-}$. The conductivity drop at higher concertation suggests that thicker solution depresses the carrier mobility.

However, the concentration trend of the solution viscosity disobeys the Jones–Dole $\eta(C) = AC + BC^{1/2}$ notion[34] or the $f_{YX2}(C)$ as compared with that for the monovalent salt solution, see Figure 6. The folded X^{-} concentration and the large amount of Y^{2+} charge lead to the X^{-}~Y^{2+} attraction that is absent in monovalent salt solutions. The short X^{-}~Y^{2+} attraction could be the origin of the viscosity disobeying Jones–Dole notion.

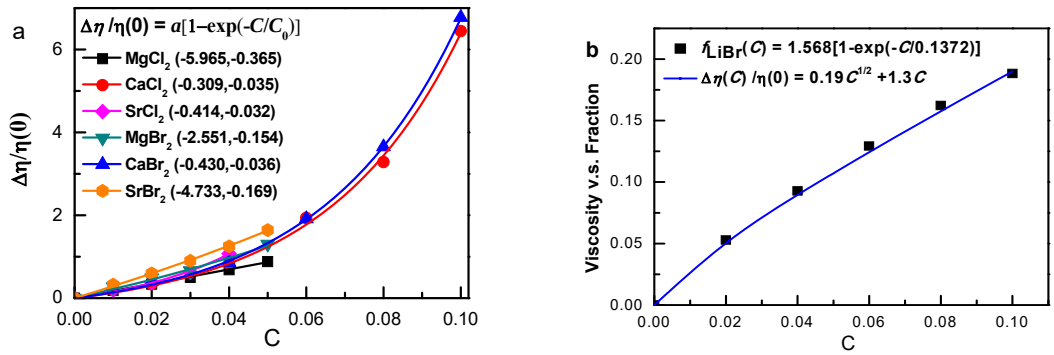

Figure 6. Solute concentration and type resolved viscosity for the (a) YX_2 and (b) LiBr [27] solutions. The viscosity of the YX_2 shows opposite curvatures to that of the monovalent salt solutions [35]. The solution viscosity, surface stress, and the $f_{LiBr}(C)$, for instance[27], follow the Jones–Dole notion[36]. The viscosity of the YX_2 solutions follow the same trend of the divalent $CaCl_2$[37] and the complex $NaClO_4$ and $LiClO_4$ [38] aqueous solutions.

5. Conclusion

The DPS strategy has enabled discrimination of the ionic roles on transforming the O:H–O bond upon charge injection by YX_2 solvation and the effect on the surface stress, solution viscosity and conductivity. We may summarize the findings:

1) The $Y^{2+} + 2X^-$ is less capable of transiting O:H–O bond stiffness than the monovalent salt solutions as the superposition of the $Y^{2+} + 2X^-$ ionic fields.
2) On the base of $f_H(C) \cong 0$ and $f_{HX}(C) \cong f_X(C)$, the $f_{YX2}(C)$ is decomposed into the coefficients $f_Y(C)$ and $f_{X2}C)$ for the Y^{2+} and $2X^-$, respectively.
3) The $f_{X2}(C) \propto 1 - \exp(-C/C_0)$ toward saturation indicates the presence of $X^- \leftrightarrow X^-$ repulsion that weakens the anionic electric field and the shell size.
4) The $f_Y(C) \propto C$ at the molecular ratio below 0.05 suggests the invariant hydration shell size; however, at higher Y concentration, the $f_Y(C)$ turns to be the similar form and the mechanism of f_{X2}(C).
5) The concentration-trend consistency of $f_{YX2}(C)$, solution conductivity, and surface stress for YX_2 solutions clarifies their common origin of ionic polarization. However, the Jones–Dole

notion disobedience of the viscosity $\eta_{YX2}(C)$ suggests the presence of Y^{2+}~X^{-} electrostatic attraction.

Acknowledgments

Financial support received from Natural Science Foundation (Nos. 11872052(YL); 21875024(CQ)), and the Science Challenge Project (No. TZ2016001) of China are acknowledged.

References

1. Lupascu, T.; Ciobanu, M.; Botan, V., Removal of Divalent Iron and Manganese Ions and Hydrogen Sulfide from Groundwater. *Chemistry Journal of Moldova* **2014,** *9* (2), 58-61.
2. Weggler, K.; Mclaughlin, M. J.; Graham, R. D., Effect of chloride in soil solution on the plant availability of biosolid-borne cadmium. *Journal of Environmental Quality* **2004,** *33* (2), 496.
3. Moss, D. M.; Siccardi, M.; Murphy, M.; Piperakis, M. M.; Khoo, S. H.; Back, D. J.; Owen, A., Divalent Metals and pH Alter Raltegravir Disposition In Vitro. *Antimicrobial Agents & Chemotherapy* **2012,** *56* (6), 3020.
4. Oztop, M. H.; Mccarthy, K. L.; Mccarthy, M. J.; Rosenberg, M., Monitoring the effects of divalent ions (Mn +2 and Ca +2) in heat-set whey protein gels. *LWT - Food Science and Technology* **2014,** *56* (1), 93-100.
5. Morgan, J. B.; Miller, R. K.; Mendez, F. M.; Hale, D. S.; Savell, J. W., Using calcium chloride injection to improve tenderness of beef from mature cows. *Journal of Animal Science* **1991,** *69* (11), 4469-4476.
6. N'Tsoukpoe, K. E.; Rammelberg, H. U.; Lele, A. F.; Korhammer, K.; Watts, B. A.; Schmidt, T.; Ruck, W. K. L., A review on the use of calcium chloride in applied thermal engineering. *Applied Thermal Engineering* **2015,** *75*, 513-531.
7. Qiu, G. H.; Wen, H.; Guo, Q.; Hu, Y. H.; Yang, D.; Liu, F., Electrochemical preparation of nanosized manganese dioxides from manganese chloride solutions. *Ionics* **2011,** *17* (3), 209.
8. Zhou, X. J.; Xia, W. T.; Yin, J. G., Extraction of Copper and Cobalt from Nickel Chloride Solution with N235. *Advanced Materials Research* **2012,** *361-363*, 615-618.
9. Time, S. T., The Influence of Calcium Chloride Salt Solution on the Transport Properties of Cementitious Materials. *Advances in Civil Engineering* **2015,** *2015* (2), 154-166.
10. Knape, M. J.; Ahuja, L. G.; Bertinetti, D.; Burghardt, N. C. G.; Zimmermann, B.; Taylor, S. S.; Herberg, F. W., Divalent Metal Ions Mg2+ and Ca2+ Have Distinct Effects on Protein Kinase A Activity and Regulation. *Acs Chemical Biology* **2015,** *10* (10), 2303.
11. Lamberts, K.; MD, Ş.; Englert, U., One- and two-dimensional polymers from proline and calcium bromide. *Acta Crystallogr C Struct Chem* **2015,** *71* (Pt 4), 311-317.
12. Hofmeister.F., Concerning Regularities in the Protein-Precipitating Effects of Salts and the Relationship of These Effects to the Physiological Behaviour of Salts. *Arch. Exp. Pathol. Pharmacol* **1888,** *24*, 247–260.
13. Perelygin, I. S.; Mikhailov, G. P.; Tuchkov, S. V., Vibrational and orientational relaxation of polyatomic anions and ion-molecular hydrogen bond in aqueous solutions *Journal of Molecular Structure* **1996,** *381* (1–3), 189-192.
14. Bruni, F.; Imberti, S.; Mancinelli, R.; Ricci, M. A., Aqueous solutions of divalent chlorides: Ions hydration shell and water structure. *Journal of Chemical Physics* **2012,** *136* (6), 137-48.
15. Kanno.H., Correlation of the Raman v1 bands of aquated divalent metal ions with the cation-hydrated water distance *Journal of Raman Spectroscopy* **1987,** *18* (4), 301-304.
16. Yamada, S. A.; Bailey, H. E.; Tamimi, A.; Li, C.; Fayer, M. D., Dynamics in a Room-Temperature Ionic Liquid from the Cation Perspective: 2D IR Vibrational Echo Spectroscopy. *Journal of the American Chemical Society* **2017,** *139* (6), 2408-2420.
17. Bakker, H. J.; Kropman, M. F.; Omta, A. W.; Woutersen, S., Hydrogen-Bond Dynamics of Water in Ionic Solutions. *Physica Scripta* **2004,** *69* (6), C14.
18. Piatkowski, L.; Bakker, H. J., Vibrational dynamics of the bending mode of water interacting with ions. *Journal of Chemical Physics* **2011,** *135* (21), 214509.
19. Ho, Y. S.; Porter, J. F.; Mckay, G., Equilibrium Isotherm Studies for the Sorption of Divalent Metal Ions onto Peat: Copper, Nickel and Lead Single Component Systems. *Water Air & Soil Pollution* **2002,** *141* (1-4), 1-33.
20. Solt, I.; Simon, I.; Császár, A. G.; Fuxreiter, M., Electrostatic versus nonelectrostatic effects in DNA sequence

discrimination by divalent ions Mg2+ and Mn2+. *Journal of Physical Chemistry B* **2007,** *111* (22), 6272-6279.

21. Lippard, S. J.; Berg, J. M., Bio-inorganic chemistry: Newly charted waters: Editorial overview. *Current Opinion in Chemical Biology* **2000,** *4* (2), 137-139.

22. Ayotte, P.; Weddle, G. H.; Jun Kim, A.; Johnson, M. A., Vibrational Spectroscopy of the Ionic Hydrogen Bond: Fermi Resonances and Ion−Molecule Stretching Frequencies in the Binary X-·H2O (X = Cl, Br, I) Complexes via Argon Predissociation Spectroscopy. *Journal of the American Chemical Society* **1998,** *120* (47), 12361-12362.

23. Kropman, M. F.; Bakker, H. J., Dynamics of water molecules in aqueous solvation shells. *Science* **2001,** *291* (5511), 2118-2120.

24. Bakker, H. J., Structural Dynamics of Aqueous Salt Solutions. *Chemical Reviews* **2008,** *108* (4), 1456-1473.

25. Cappa, C. D.; Smith, J. D.; Messer, B. M.; Cohen, R. C.; Saykally, R. J., Effects of cations on the hydrogen bond network of liquid water: new results from X-ray absorption spectroscopy of liquid microjets. *Journal of Physical Chemistry B* **2006,** *110* (11), 5301-5309.

26. Jong, P. H. K. D.; Neilson, G. W.; Bellissent‐Funel, M. C., Hydration of Ni2+ and Cl− in a concentrated nickel chloride solution at 100 °C and 300 °C. *Journal of Chemical Physics* **1996,** *105* (12), 5155-5159.

27. Sun, C. Q.; Chen, J.; Gong, Y.; Zhang, X.; Huang, Y., (H, Li)Br and LiOH Solvation Bonding Dynamics: Molecular Nonbond Interactions and Solute Extraordinary Capabilities. *Journal of Physical Chemistry B* **2018,** *122* (3), 1228.

28. Liu, X.; Xi, Z.; Bo, M.; Lei, L.; Tian, H.; Nie, Y.; Yi, S.; Xu, S.; Yan, W.; Zheng, W., Coordination-Resolved Electron Spectrometrics. *Chemical Reviews* **2015,** *115* (14), 6746.

29. Huang, Y.; Zhang, X.; Ma, Z.; Zhou, Y.; Zheng, W.; Zhou, J.; Sun, C. Q., Hydrogen-bond relaxation dynamics: Resolving mysteries of water ice. *Coordination Chemistry Reviews* **2015,** *285*, 109-165.

30. Zhang, X.; Zhou, Y.; Gong, Y.; Huang, Y.; Sun, C., Resolving H(Cl, Br, I) capabilities of transforming solution hydrogen-bond and surface-stress. *Chemical Physics Letters* **2017,** *678*, 233-240.

31. Zhang, X.; Xu, Y.; Zhou, Y.; Gong, Y.; Huang, Y.; Sun, C. Q., HCl, KCl and KOH solvation resolved solute-solvent interactions and solution surface stress. *Applied Surface Science* **2017,** *422* (15), 475-481.

32. Wang, S.; Zhang, X.; Liu, Y.; Huang, Y.; Sun, C. Q., Antimonene Nanoribbon Band-Gap Expansion: Bond Contraction and Edge Quantum Entrapment. *Materials Chemistry & Physics* **2018,** *211*, 414-419.

33. Zhou, Y.; Gong, Y.; Huang, Y.; Ma, Z.; Zhang, X.; Sun, C. Q., Fraction and stiffness transition from the H O vibrational mode of ordinary water to the HI, NaI, and NaOH hydration states. *Journal of Molecular Liquids* **2017,** *244*, 415-421.

34. Jones, G.; Dole, M., The viscosity of aqueous solutions of strong electrolytes with special reference to barium chloride. *Journal of the American Chemical Society* **1929,** *51* (10), 2950-2964.

35. Zhou, Y.; Huang, Y.; Ma, Z.; Gong, Y.; Zhang, X.; Sun, Y.; Sun, C. Q., Water molecular structure-order in the NaX hydration shells (X= F, Cl, Br, I). *Journal of Molecular Liquids* **2016,** *221*, 788-797.

36. Jones, G.; Dole, M., The viscosity of aqueous solution of strong electrolytes with special reference to barium chloride. *Journal of the American Chemical Society* **1929,** *51* (10), 2950-2964.

37. Lide, D. R., *CRC Handbook of chemistry and physics, 80th Ed.* CRC Press Boca Raton, 1999.

38. Wei, Q.; Zhou, D.; Bian, H., Negligible cation effect on the vibrational relaxation dynamics of water molecules in NaClO 4 and LiClO 4 aqueous electrolyte solutions. *RSC Advances* **2017,** *7* (82), 52111-52117.